EurJOC
European Journal of Organic Chemistry

Full Papers
doi.org/10.1002/ejoc.202001469

Chemistry Europe
European Chemical Societies Publishing

Computational and Experimental Insights into Asymmetric Rh-Catalyzed Hydrocarboxylation with CO_2

Ljiljana Pavlovic,[a] Martin Pettersen,[b] Ashot Gevorgyan,[b] Janakiram Vaitla,[b] Annette Bayer,*[b] and Kathrin H. Hopmann*[a]

The asymmetric Rh-catalyzed hydrocarboxylation of α,β-unsaturated carbonyl compounds was originally developed by Mikami and co-workers but gives only moderate enantiomeric excesses. In order to understand the factors controlling the enantioselectivity and to propose novel ligands for this reaction, we have used computational and experimental methods to study the Rh-catalyzed hydrocarboxylation with different bidentate ligands. The analysis of the C–CO_2 bond formation transition states with DFT methods shows a preference for outer-sphere CO_2 insertion, where CO_2 can undergo a backside or frontside reaction with the nucleophile. The two ligands that prefer a frontside reaction, StackPhos and ^{t}Bu-BOX, display an intriguing stacking interaction between CO_2 and an N-heterocyclic ring of the ligand (imidazole or oxazoline). Our experimental results support the computationally predicted low enantiomeric excesses and highlight the difficulty in developing a highly selective version of this reaction.

Introduction

Widespread efforts are currently devoted to the search of catalysts, which can fixate CO_2 into organic molecules.[1] A significant part of this activity is focused on metal-catalyzed carbon-carbon bond formation with CO_2.[2] For the metal-catalyzed formation of saturated carboxylic acids, different protocols have been reported, including carboxylation of halides (C–X bonds)[2a,b] and reductive carboxylation of unsaturated compounds such as alkenes.[2c–h] An example of the carboxylation of Csp^3–X bonds has been reported by Martin and co-workers, who developed a mild Ni(I)-catalyzed protocol for converting benzyl halides and CO_2 to phenylacetic acids.[2b] The catalytic reductive carboxylation of alkenes is a challenging area, which has witnessed some progress in recent years. For example, Greenhalgh and Thomas reported a Fe(II)-catalyzed synthesis of α-aryl carboxylic acids from styrene derivatives and CO_2.[2e] A Cu(I)/CsF-based protocol for the incorporation of CO_2 into disubstituted alkenes was reported by Skrydstrup, Nielsen, and co-workers.[2h]

Interestingly, many of the known C–CO_2 bond formations result in generation of *chiral* carboxylic acids, but as racemic mixtures only.[2b,e,h] Indeed, the design of enantioselective C–CO_2 bond formation reactions remains a major challenge. This is demonstrated by the fact that only very few studies on asymmetric C–CO_2 bond formation have been reported.[1f,2c,3] In order to broaden the usefulness of CO_2 as a carbon synthon in the chemical and pharmaceutical industry, it is essential that novel enantioselective carboxylation protocols are developed, for example for the preparation of chiral carboxylic acids, which are important intermediates in many synthetic processes.[4]

A promising asymmetric C–CO_2 bond formation protocol has been reported by Mikami and co-workers in 2016, involving the first enantioselective hydrocarboxylation of α,β-unsaturated carbonyl compounds (Figure 1).[2c] The rhodium-based reaction involved the use of (*S*)-SEGPHOS as a chiral ligand, but only moderate enantiomeric excesses (*e.e.*'s) of up to 66% could be

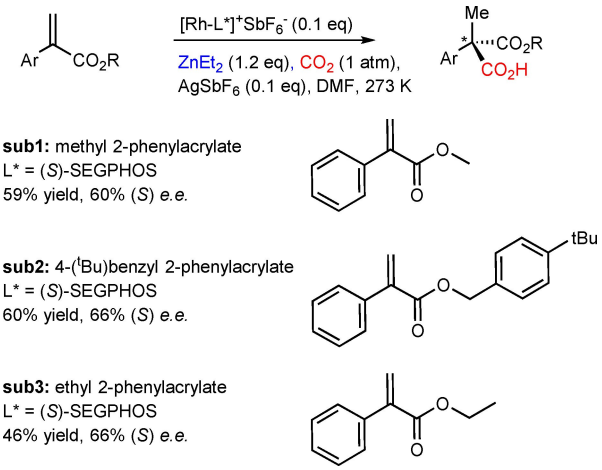

Figure 1. Enantioselective hydrocarboxylation reaction reported by Mikami and coworkers.[2c]

[a] *Dr. L. Pavlovic, Prof. Dr. K. H. Hopmann*
Hylleraas Center for Quantum Molecular Sciences
Department of Chemistry, UiT The Arctic University of Norway
9037 Tromsø, Norway
E-mail: kathrin.hopmann@uit.no
https://site.uit.no/choco
[b] *M. Pettersen, Dr. A. Gevorgyan, Dr. J. Vaitla, Prof. Dr. A. Bayer*
Department of Chemistry, UiT The Arctic University of Norway
9037 Tromsø, Norway
E-mail: annette.bayer@uit.no
https://site.uit.no/bayerlab/

Supporting information for this article is available on the WWW under https://doi.org/10.1002/ejoc.202001469

achieved.[2c] The (*S*)-BINAP ligand gave similar results to (*S*)-SEGPHOS whereas other ligands, such as (*S*)-SynPhos or (*R*,*R*)-^{i}Pr-DuPhos, provided significantly lower *e.e.*'s.[2c]

A computational analysis of the related non-enantioselective Rh-COD-catalyzed hydrocarboxylation reaction showed that during C–CO_2 bond formation, the CO_2 molecule does not interact with rhodium.[5] Moreover, it was shown that benzylic substrates display an unusual η^6-coordination mode, with the nucleophilic carbon positioned up to 3.6 Å away from rhodium.[5] The same substrate binding mode and preference for an outer sphere CO_2 insertion were found computationally for the chiral Rh-(*S*)-SEGPHOS catalyst.[6] This raises the question how the enantioselectivity is controlled in systems where CO_2 is not constrained through interactions with the metal. Although CO_2 preferably is positioned in the outer sphere, it may still be affected by repulsive and attractive nonbonding interactions with the ligand. A better understanding of the factors that govern the preferred positions and orientations of CO_2 may help to design catalysts with higher enantioselectivities.

Modern computational methods are sufficiently advanced to provide insights into the factors that control the enantioselectivity in metal-catalyzed reactions.[7] For example, the selectivity may be influenced by the presence of specific interactions between the chiral catalyst and the substrate, and in particular, nonbonding forces may contribute significantly to the preferred formation of one product enantiomer.[7–8] The identification of the selectivity-determining interactions typically relies on the computational optimization of the involved diastereomeric transition states. Such structures are generally built manually, followed by DFT optimizations, using different optimization algorithms.[9] However, approaches to speed-up the computational analysis through automatized techniques have been put forward,[10] with one example being the open-source toolkit AARON (An Automated Reaction Optimizer for New catalysts) designed by Wheeler and co-workers.[10a] AARON employs TS templates provided by the user, but can automatically swap the ligands to build new geometries.

Herein, we perform a computational analysis of the selectivity-determining factors in the Rh-catalyzed hydrocarboxylation for four chiral rhodium complexes, of which three ligands have not previously been tested in this reaction. Ligand swapping is performed with AARON, followed by DFT optimizations. To validate the enantioselectivities predicted by the computations, an experimental analysis of all systems is performed.

Results and Discussion

Our study of the Rh-catalyzed asymmetric hydrocarboxylation reaction consists of three parts. Initially, we validated the computational protocol through analysis of the Rh-(*S*)-SEGPHOS-catalyzed hydrocarboxylation of two experimentally known substrates.[2c] Next, we expanded our computational study to include the CO_2 insertion TSs for three additional chiral ligands, which have not been used in experiments on this reaction. Finally, we conducted an experimental evaluation of the corresponding Rh-complexes for hydrocarboxylation of ethyl 2-phenylacrylate.

For the analysis of the chiral ligands, 10 outer sphere CO_2 insertion TSs were built for each ligand, with different ligand-substrate orientations (Figure 2). Five of them were pro-(*S*)-TSs, and five the corresponding pro-(*R*) TSs. In the conformations **TS1a** and **TS1b**, the phenyl ring of the substrate interacts with the Rh-center in an η^6 fashion, whereas CO_2 is in the outer sphere, leading to a *backside* C–CO_2 bond formation (reminiscent of a S_E2(back) reaction). The difference between **TS1a** and **TS1b** is the orientation of the ester moiety (Figure 2). At **TS2a** and **TS2b**, the substrate is still bound in an η^6 fashion, but the CO_2 is positioned closer to metal, leading to a *frontside* reaction (reminiscent of a S_E2(front) reaction). At **TS3**, both the phenyl group and the carbonyl oxygen of the substrate interact with the Rh-center. It is important to highlight that for the comparative analysis of the four ligands, only *outer sphere* CO_2 insertion was considered,[5] because the TS conformations, where interactions between Rh and CO_2 take place (referred to as *inner sphere* CO_2 insertion), show very high barriers (TS4_S and TS4_R, Supporting Information, Table S1). The four studied chiral ligands are given in Figure 3.

Computational analysis of Rh-(*S*)-SEGPHOS: The Rh-SEGPHOS-catalyzed hydrocarboxylation was here investigated computationally with the styrene-type α,β-unsaturated carbonyl substrates **sub1** and **sub2** (Figure 1), which previously have been studied experimentally by Mikami and co-workers.[2c] The overall hydrocarboxylation mechanism for substrates of this type has been reported with $[Rh(cod)Cl]_2$ (SI, Figure S1).[5] We have here studied the full mechanism with Rh-(*S*)-SEGPHOS as the catalyst and methyl 2-phenylacrylate (**sub1**) as the substrate, with the energy profile shown in Figure S2 (Supporting Information). The mechanistic steps include a transmetallation of an ethyl from diethylzinc to the precatalyst, followed by a β-hydride elimination to give an Rh-H-Et intermediate. Insertion

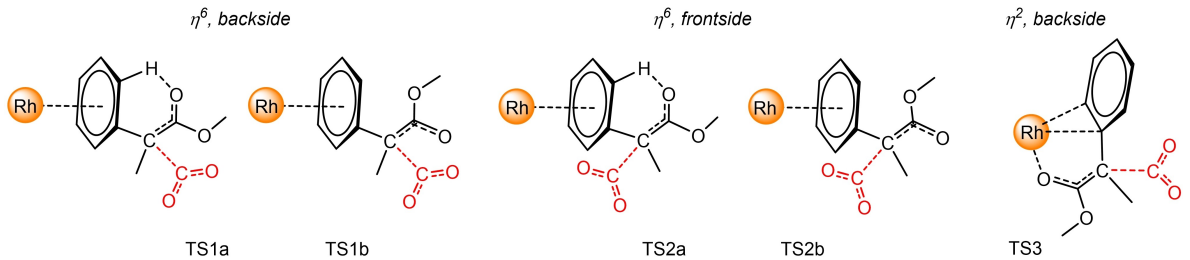

Figure 2. Five TS orientations considered here. For each of these, both pro-(*R*) and pro-(*S*) conformations were included.

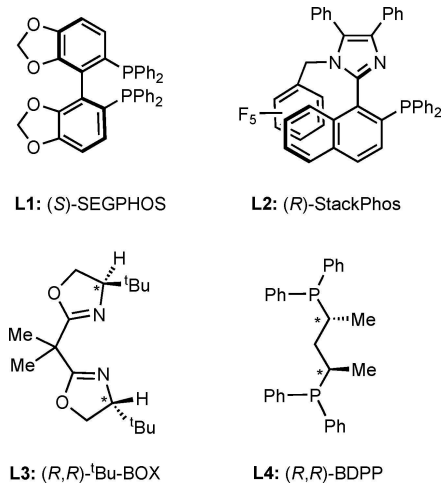

Figure 3. Four chiral ligands studied here in Rh-catalyzed hydrocarboxylation.

of the substrate leads to an energetically low-lying Rh-benzyl species that can attack CO_2.[5] The CO_2 insertion is rate- and enantioselectivity-determining.[5] At the carboxylation TS, the benzyl group prefers to coordinate in an η^6 mode to rhodium, with the formally negative charge on the substrate delocalized between the nucleophilic carbon and the ester group, yielding an intermediate enolate (Figure 4). The enolate can attack CO_2 from its *re* or *si* face, and with a chiral ligand, unequal amounts of the (*R*)- and (*S*)-enantiomer of the product can be formed.

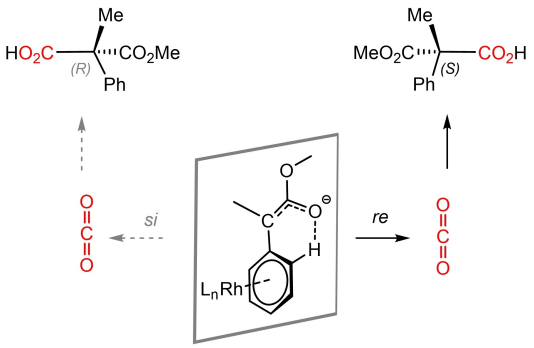

Figure 4. Illustration of the enolate intermediate of **sub1** and its attack on CO_2.

Carboxylation of methyl 2-phenylacrylate: In order to validate our computational protocol and our mechanistic understanding of this reaction, we first analyzed the Rh-(*S*)-SEGPHOS-catalyzed C–CO_2 bond formation with **sub1** (Figure 1). The results support our previous observation that CO_2 prefers to be in the outer sphere during C–CO_2 bond formation,[5] as the inner and outer sphere TSs with Rh-(*S*)-SEGPHOS show an energy difference of 17.3 kcal/mol in favor of outer-sphere insertion (SI, Table S1, Figure S3).

At the lowest-lying outer sphere transition state **TS1a_S$_{sub1/L1}$**, the η^6-coordinated enolate attacks CO_2 via its *re* face ($\triangle G^{\neq}$ = 12.1 kcal/mol relative to the Rh-benzyl intermediate, Figure S4, SI) and the experimentally observed (*S*)-product is obtained. At **TS1a_R$_{sub1/L1}$**, which is higher in energy by 0.7 kcal/mol, CO_2 is attacked by the enolate *si* face, giving the (*R*)-product (Figure 5). Other outer sphere conformations (Figure 2) were significantly higher in energy (Table 1). On the basis of all computed TS energies, we evaluated the *e.e.* for the Rh-(*S*)-SEGPHOS-catalyzed hydrocarboxylation of **sub1**, providing a computed *e.e.* of 53.8% (*S*), in very good agreement with the experimentally reported *e.e.* of 60.0% (*S*).[2c]

Various noncovalent interactions between the ligand and **sub1** can be identified at the two energetically lowest-lying SEGPHOS TSs, **TS1a_S$_{sub1/L1}$**, and **TS1a_R$_{sub1/L1}$** (Figure 5). At **TS1a_S$_{sub1/L1}$**, the phenyl rings of SEGPHOS form two C–H···π interactions (2.95, 3.10 Å) with the phenyl of the substrate. At the energetically higher lying **TS1a_R$_{sub1/L1}$**, SEGPHOS forms three C–H···π interactions with **sub1**, two with the substrate phenyl (2.97 and 3.14 Å), and one with the methyl group of the ester moiety (3.16 Å, Figure 5). As the strength of these C–H···π interactions appear similar at the two diastereomeric TSs, they do not seem to determine the selectivity. An analysis of C–H···O attractions at the two TSs shows comparable distances for interactions within the substrate (**TS1a_S$_{sub1/L1}$**: 2.16 Å, **TS1a_R$_{sub1/L1}$**: 2.11 Å), but significant differences in the *intermolecular* C–H···O interaction between the **sub1** carbonyl and the SEGPHOS phenyl (**TS1a_S$_{sub1/L1}$**: 2.46 Å, **TS1a_R$_{sub1/L1}$**: 3.00 Å). We speculate that this C–H···O interaction may be an essential factor in determining the enantioselectivity in the Rh-(*S*)-SEGPHOS-catalyzed hydrocarboxylation of methyl 2-phenylacrylate.

If CO_2 is placed closer to rhodium, here referred to as *frontside* insertion (TS2, Figure 2), the barriers increase by several kcal/mol (Figure 5). Interestingly, the *frontside* attack provides an incorrect enantioselectivity, as the **TS2a R$_{sub1/L1}$**

Table 1. Barrier differences ($\Delta\Delta G^{\neq}$, kcal/mol, 273 K) for different TS conformations (Figure 2) in Rh-catalyzed hydrocarboxylation of **sub1**.

Ligand	η^6, backside				η^6, frontside				η^2, backside		e.e.$_{comp}$	e.e.$_{exp}$
	TS1a_S	TS1a_R	TS1b_S	TS1b_R	TS2a_S	TS2a_R	TS2b_S	TS2b_R	TS3_S	TS3_R	[%]	[%]
L1 (SEGPHOS)	**0.0**	**0.7**	3.1	2.0	6.5	4.0	7.3	4.9	8.3	7.9	53.8 (S)	60.0 (*S*)[c]
L2 (StackPhos)	2.2	2.8	2.1	3.0	**0.0**[a], 0.8[b]	**0.6**,[a] 1.9[b]	0.8	1.0	15.2	10.8	47.0 (*S*)	n.d.[d]
L3 (^{t}Bu-BOX)	1.9	0.7	3.1	0.8	**0.0**	**0.5**	3.6	2.5	3.2	5.3	6.4 (*S*)	(0)[e]
L4 (BDPP)	**0.5**	**0.0**	0.8	1.9	5.8	5.5	8.6	6.4	9.7	12.1	24.3 (*R*)	(4)[e]

[a] TS2a structures as given in Figure 8 (**TS2a_S$_{sub1/L2}$**/**TS2a_R$_{sub1/L2}$**). [b] TS2a structures with stacking of pentafluorophenyl and phenyl as given in the SI, Figure S6 (**TS2a_stack S$_{sub1/L2}$**/**TS2a_stack_R$_{sub1/L2}$**). [c] From ref.[2c]. [d] Only racemic StackPhos could be tested, and the e.e. could thus not be determined. [e] Experimental results obtained here with **sub3**, which has an ethyl group instead of the methyl in **sub1** (Figure 1).

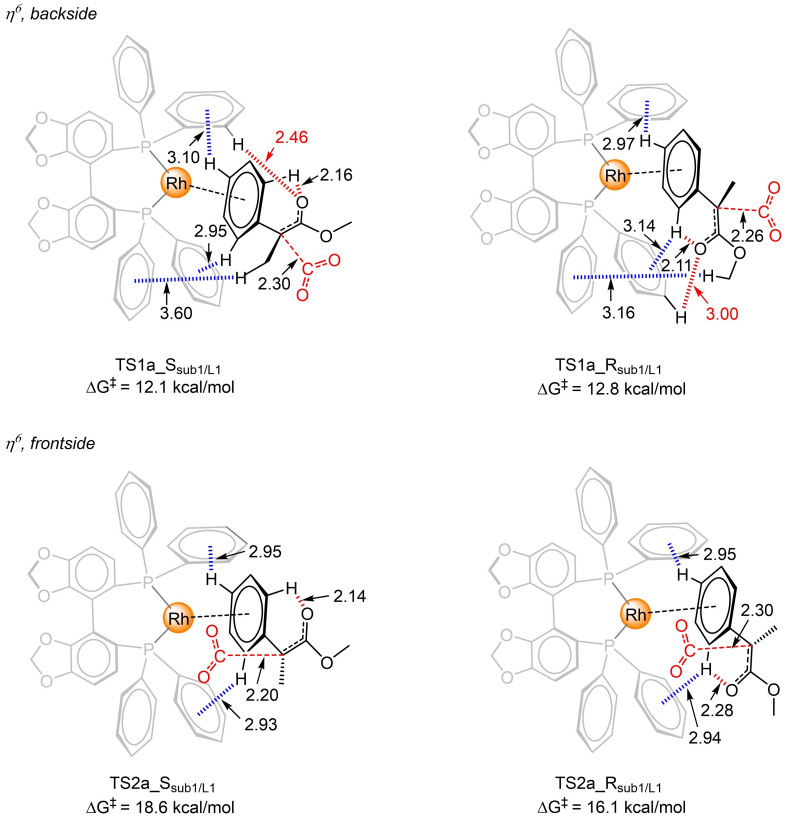

Figure 5. Illustration of the noncovalent interactions at four of the optimized CO_2 insertion TSs for Rh-(*S*)-SEGPHOS-catalyzed hydrocarboxylation of methyl 2-phenylacrylate (**sub1**). Only some of the hydrogens are shown for clarity. Distances in Å.

structure is 2.5 kcal/mol lower in energy than **TS2a S$_{sub1/L1}$**. The experimentally observed (*S*)-selectivity[2c] is thus dominated by the *backside* structures. These findings highlight the need to compare computationally predicted TSs with experimental selectivities to evaluate if appropriate TS conformations were located.

The TS3 conformations, where the ester of the substrate interacts with rhodium (Figure 2), are ~8 kcal/mol higher in energy than TS1 and are not considered relevant (Table 1).

Carboxylation of 4-(tert-butyl)benzyl 2-phenylacrylate: We proceeded to analyze **sub2**, which contains two phenyl rings (Figure 1), leading to several favorable C–H···π interactions during C–CO_2 bond formation (Figure 6). A similar pattern as for **sub1** is observed, where at the lowest-lying transition state **TS1a_S$_{sub2/L1}$** ($\triangle G^{\neq} = 12.0$ kcal/mol), the Rh-benzyl (SI, Figure S4) attacks CO_2 from its *re* face, resulting in the (*S*)-product. A favorable C–H···O (2.47 Å) interaction is seen at **TS1a_S$_{sub2/L1}$** but lacks at **TS1a_R$_{sub2/L1}$**, which is higher in energy by 1.0 kcal/mol. The computed *e.e.* of 73% (*S*) is in good agreement with the experimental value of 66% (*S*).[2c]

The combined results for **sub1** and **sub2** indicate that the enantioselectivity of Rh-(*S*)-SEGPHOS-catalyzed hydrocarboxylation appears to be a result of favorable C–H···O interactions between the substrate and the SEGPHOS ligand. At the preferred TS1a conformations (Figure 5 and Figure 6), the CO_2 molecule is placed away from the metal center (> 5 Å) and thus

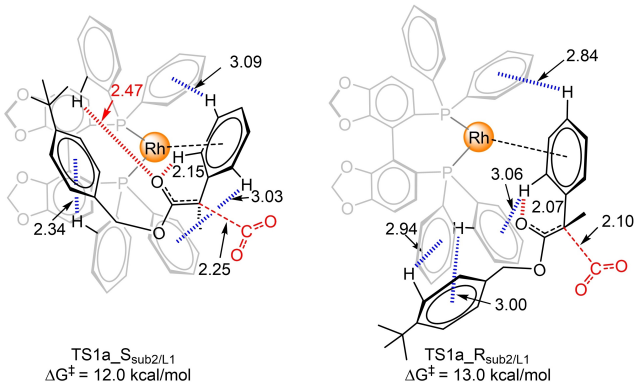

Figure 6. Illustration of the preferred TSs for Rh-(*S*)-SEGPHOS-catalyzed carboxylation of **sub2**. Only some of the hydrogens are shown for clarity. Distances in Å.

the chiral catalyst is promoting the enantioselectivity through the positioning of the alkene substrate, not through interactions with CO_2.

Potential of other ligands in the Rh-catalyzed asymmetric hydrocarboxylation: We selected a set of ligands structurally different from SEGPHOS from the library of AARON[10a] (**L2**–**L4**, Figure 3) and investigated their predicted enantioselectivities with DFT. The set includes one *P*,*N* ligand (**L2**: StackPhos),[11] an *N*,*N* ligand (**L3**: ^{t}Bu-BOX)[12] and a *P*,*P* ligand (**L4**: BDPP).[13] These

ligands have shown good performance in other asymmetric transformations (allylation, aziridination, hydrovinylation),[14] and to our knowledge, they have not previously been used for Rh-catalyzed hydrocarboxylation.

The outer sphere TS conformations depicted in Figure 2 were evaluated for **L2**–**L4** and **sub1** through manual DFT calculations, with the energies summarized in Table 1 (geometric parameters are shown in Figure 7, Figure 8 and Tables S1–4, SI). For BDPP (**L4**), we see a similar behaviour as for SEGPHOS, with a preference for *backside* insertion (Table 1). However, the StackPhos (**L2**) and ^{t}Bu-BOX (**L3**) ligands show a computed preference for *frontside* insertion. Both ligands display an intriguing stacking interaction between CO_2 and the N-heterocyclic ring of the ligand (imidazole or oxazoline, Figure 7, SI, Figure S7).

It can be noted that related attractive stacking interactions have been predicted in computational studies focusing on the binding of CO_2 to N-heterocyclic compounds,[15] and in experimental and computational studies on the solvation of aromatic compounds in supercritical CO_2.[16] However, to our knowledge, the heterocycle-CO_2 stacking interaction has not been described in the context of an organometallic ligand or a CO_2 insertion reaction.

The heterocycle-CO_2 interaction appears strongest at the StackPhos TS geometries, with a nitrogen-C_{CO2} distance of 3.22 Å (Figure 7). The StackPhos TS geometries with **sub1** are therefore discussed in further detail here. Besides the CO_2-imidazole stacking, the lowest lying **TS2a_S**$_{sub1/L2}$ also displays an intriguing F-π attraction between a fluoro group of the pentafluoro-phenyl and the naphthalene ring (3.05 Å), alongside a C–H···F interaction (2.53 Å, Figure 8). Similar F-π interactions to phenantrene-like aromatic systems have been reported in the literature.[17] Interestingly, this F-π interaction is not seen in the X ray structure of the StackPhos ligand,[11a] which instead displays π-π stacking between pentafluorophenyl and naphthalene subunits (3.38 Å). In our computations, this π-π stacking increases the TS energy by 2.5 kcal/mol (SI, Figure S5).

An alternative π-π interaction between pentafluorophenyl and another phenyl substituent increases the CO_2 insertion barrier slightly by 0.8 kcal/mol (**TS2a_stack_S**$_{sub1/L2}$ SI, Figure S6). In the case of *backside* insertion with StackPhos, the imidazole-CO_2 interactions are absent, which increases the barriers by 2 to 3 kcal/mol (Table 1). The TS3 structures, where the ester carbonyl interacts with rhodium, are more than 11 kcal/ mol above the TS2 structures and therefore are not relevant.

The best (*R*)-pathway obtained for **sub1** with StackPhos proceeds via *frontside* insertion and is 0.6 kcal/mol above the best (*S*)-structure (**TS2a_R**$_{subl/L2}$, Figure 8). This TS also displays stacking of CO_2 above the imidazole moiety and an F-π interaction between pentafluorophenyl and the naphthalene subunits (Figure 8). The *e.e.* computed on the basis of all obtained StackPhos TS structures is 47 % (*S*) (Table 1), which indicates that this ligand is not expected to perform significantly better than SEGPHOS.

The other studied ligands are predicted to give low *e.e.*'s. Our calculations show that with the (*R*,*R*)-^{t}Bu-BOX chiral ligand, at the lowest-lying **TS2a S** $_{sub1/L3}$, the *frontside* CO_2 insertion is preferred (SI, Figure S7). The opposite enantiomer **TS2a R** $_{sub1/L3}$ is higher in energy by only 0.5 kcal/mol. The predicted *e.e.* on the basis of all optimized TS conformations is only 6.4 % (Table 1).

With the (*R*,*R*)-BDPP ligand, at the lowest-lying **TS1a R** $_{sub1/L4}$, the CO_2 prefers *backside* insertion (SI, Figure S7). **TS1a_S** $_{sub1/L4}$ has a barrier that is only 0.5 kcal/mol higher than **TS1a_R** $_{sub1/L4}$.

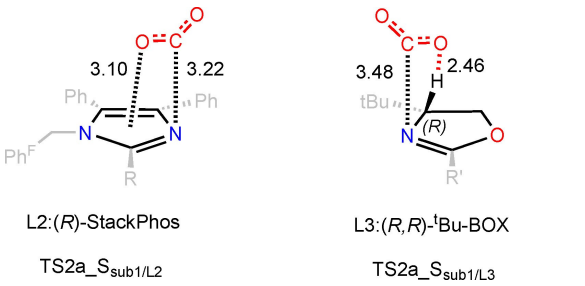

Figure 7. Stacking of CO_2 above the N-heterocyclic ring of **L2** and **L3** at the *frontside* TSs. Distances in Å.

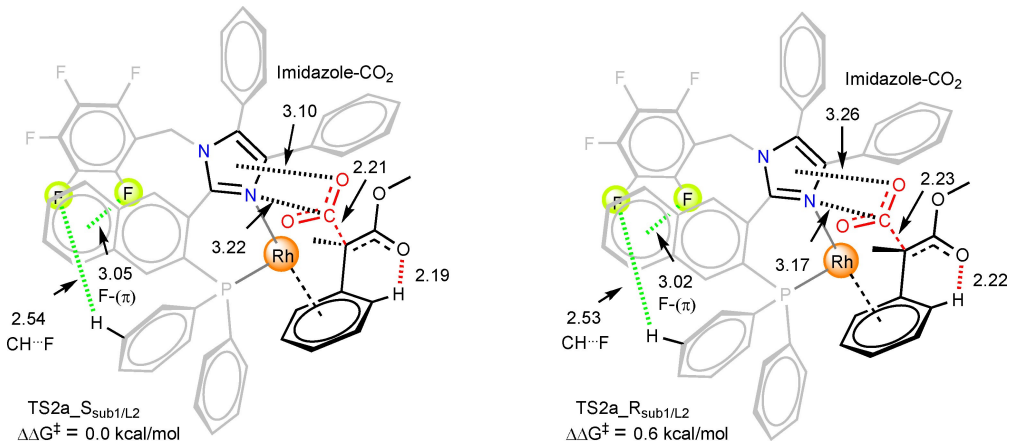

Figure 8. Illustration of the preferred TSs for Rh-(*R*)-StackPhos-catalyzed carboxylation of **sub1**. Distances in Å

The TSs for the *frontside* CO_2 insertion are higher in energy by more than 5 kcal/mol (Table S4). This scenario is reminiscent of the biphospine ligand (*S*)-SEGPHOS. These observations may be a consequence of the bulky phenyl groups of the ligands, which restrict CO_2, making the *backside* insertion more preferable. The computed *e.e.* for this ligand is 24% (*R*) (Table 1).

Experimental analysis of Rh-catalyzed hydrcarboxylation of L1 to L4: We analyzed the ability of **L1** to **L4** to mediate the CO_2 insertion reaction with **sub3** (Figure 1), which is closely related to the computationally studied substrate **sub1**, but which has an ethyl instead of a methyl ester. In the work by Mikami and co-workers, **sub3** and **sub1** behaved similarly, providing respectively 66% and 60% *e.e.'s* for Rh-SEGPHOS catalyzed hydrocarboxylation.[2c]

In our work, we obtained a product yield of 48% and an *e.e.* of 32% with **L1** and **sub3** (Table 2). Although the yield is similar as previously reported, the *e.e.* is somewhat lower than the reported 66%.[2c] For **L2**, only a racemic mixture of the ligand could be tested,[18] providing a yield of 74% for carboxylation of **sub3** (Table 2). Thus, **L2** may provide reasonable yields, and may be a relevant starting point for future development of ligands for this reaction.

For **L3**, experimental hydrocarboxylation of **sub3** gave the acid in as much as 99% yield but with 0% *e.e.* (Table 2), in good agreement with our predictions for **sub1** of 6.4% *e.e.* (Table 1).

For **L4**, our experimental results on **sub3** showed 94% yield, but only 4% *e.e.* (Table 2), in line with the predicted low *e.e.* of 24% *e.e.* for **sub1** (Table 1).

We conclude that our experimental results are in good agreement with the low *e.e.*'s predicted by the computations. This validates the proposed outer sphere mechanisms presented here for ligands **L1** to **L4** and indicates that DFT-D methods can be employed to model the enantioselectivities of these kinds of systems. At the same time, it highlights the difficulty to make a selective version of the rhodium-catalyzed hydrocarboxylation of acrylates.

Conclusion

We have employed computational and experimental methods to study the potential of bidentate chiral ligands **L1** to **L4** for the asymmetric rhodium-catalyzed hydrocarboxylation of acrylates.

Our DFT analysis of the mechanism supports a preference for an η^6 coordination of benzylic substrates and an outer sphere insertion of CO_2 also with chiral ligands.[5] The reported experimental enantioselectivity with SEGPHOS[2c] is reproduced for substrates **sub1** and **sub2** in our calculations and is predicted to arise from the C–H···O interaction between a phenyl group of SEGPHOS and the carbonyl group of the substrate.

Our computations on the chiral *P,N* ligand StackPhos (**L2**), the *N,N* ligand ^{t}Bu-BOX (**L3**) and the *P,P* ligand BDPP (**L4**) showed up to 47% *e.e.* for **sub1**. For StackPhos and ^{t}Bu-BOX, the preferred transition state geometries display an intriguing stacking interaction of CO_2 with the N-heterocyclic ring (imidazole or oxazoline, Figure 7). Experimental analyses of ligands **L1** to **L4** showed that all are able to catalyze the hydrocarboxylation reaction, with **L2, L3**, and **L4** providing good yields of 74 to 99% for carboxylation of **sub3**. Although the experimentally observed enantiomeric excesses are low, they are in good agreement with computations, underpinning the ability of DFT-D to adequately model complex enantioselective reactions.

Our combined results on Rh-catalyzed hydrocarboxylation indicate that the enantioselectivity of this reaction is difficult to control. A possible strategy to be considered is to steer CO_2 into a specific position to decrease its conformational freedom. The noncovalent stacking interactions observed between CO_2 and **L2** or **L3** (Figure 7) may be interesting in this sense and variants of these ligands may thus be a relevant starting point for future developments.

Table 2. Experimental yields and e.e's with four chiral ligands employed in Rh-catalyzed hydrocarboxylation of **sub3**.

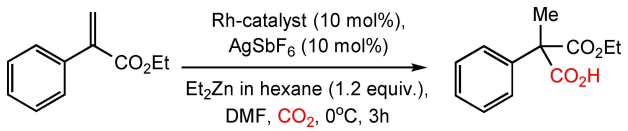

Ligand	Yields [%]	e.e.$_{exp}$ [%]
L1 (SEGPHOS)	48.0	32.0
L2 (StackPhos)	74.0	n.d.[a]
L3 (^{t}Bu-BOX)	99.0	0.0
L4 (BDPP)	94.0	4.0

[a] n.d = Not detected.

Computational section

Computational models: Calculations were performed with full substrates **sub1** and **sub2** (Figure 1) and with the full ligands (Figure 3). No molecular truncations or symmetry constraints were applied.

Computational methods: All calculations were performed at the DFT level of theory as implemented in the Gaussian09 package.[19] For geometry optimizations, the DFT functional PBE[20] was employed together with the Grimme empirical dispersion correction (D2[21]) and the implicit polarizable continuum model using the integral equation formalism, IEFPCM[22] (DMF solvent). The PBE functional has been found to be an adequate choice for rhodium-catalyzed hydrocarboxylation reactions in our previous study,[5] where it provided a good agreement with experimental results.[2c] The geometries of all intermediates and transition states were fully optimized and frequency calculations were performed in order to confirm the nature of the stationary points, where all transition states structures exhibited only one imaginary frequency.

In geometry optimizations, the BS1 basis set was employed, consisting of 6-311G(d,p)[23] for C, H, O, N, F, and P, and the LANL2DZ[24] basis set and pseudopotential for rhodium, including an extra f polarization function with exponent 1.35.[25] A larger basis set, BS2, was employed for single-point energy calculations, consisting of 6-311 + G(2d,2p) on all non-metal atoms and LANL2TZ (f) on rhodium.

In order to convert computed free energies (ΔG°, BS1) at 1 atm into a 1 M standard state, a standard state (SS) correction was included. At 273 K, this correction is −1.69 kcal/mol (for a reaction that goes from 2 moles to 1).[26]

The final Gibbs free energy was determined with the following expression: $\Delta G^\circ_{1M,273K} = \Delta G^\circ_{1atm,BS1,273K} - \Delta E_{BS1} + \Delta E_{BS2} + SS_{273K}$.

The enantiomeric excess (*e.e.*) was computed using the formula Eq. (1):[7,27]

$$e.e.(\%) = \frac{\sum_{i=1}^{n} k_{Ri} - \sum_{i=1}^{n} k_{Si}}{\sum_{i=1}^{n} k_{Ri} + \sum_{i=1}^{n} k_{Si}}$$

where k_{Ri} are the computed rate constants of TS structures with (*R*) configuration, which are summed from i = 1 to i = n, where n is equal to the number of TSs within 3 kcal/mol from the best TS. k_{si} is the equivalent for (*S*)-TSs.

AARON ligand swapping: The TS library used for AARON[10a] was based on the SEGPHOS structures obtained in the manual DFT analysis. Three ligands present in the AARON ligand library (**L2, L3, L4**) were then specified to be swapped with SEGPHOS. We preoptimized the conformations with the swapped ligands with AARON in two steps, using HF/6-31 in the first step and PBE-D2/$BS1_{mod}$ in the second step, where $BS1_{mod}$ is as BS1 but lacks the additional f polarization function on rhodium, as AARON did not allow the addition of basis functions. The obtained geometries for all ligands were then used as input for further manual DFT investigations, with the protocol as described above for manual DFT calculations. Note that for **L4**, the (*R*,*R*) ligand was computed, but the (*S*,*S*) ligand was used in experiments (which should give opposite enantioselectivity).

Experimental Section

Experimental Details: Commercially available starting materials, reagents, catalysts, and anhydrous and degassed solvents were used without further purification. Thin-layer chromatography was carried out using Merck TLC Silica gel 60 F_{254} and visualized by short-wavelength ultraviolet light or by treatment with potassium permanganate ($KMnO_4$) stain. ^1H, ^{13}C, ^{19}F, and ^{31}P NMR spectra were recorded on a Bruker Avance 400 MHz at 20 °C. All ^1H NMR spectra are reported in parts per million (ppm) downfield of TMS and were measured relative to the signals for $CHCl_3$ (7.26 ppm). All ^{13}C NMR spectra were reported in ppm relative to residual $CDCl_3$ (77.20 ppm) and were obtained with ^1H decoupling. Coupling constants, *J*, are reported in Hertz (Hz). High-resolution mass spectra (HRMS) were recorded from methanol solutions on an LTQ Orbitrap XL (Thermo Scientific) in positive electrospray ionization (ESI) mode.

(*S*)-SEGPHOS, (*S*,*S*)-^{t}Bu-BOX, and (*S*,*S*)-BDPP ligands are commercially available. Ethyl 2-phenylacrylate, StackPhos, and corresponding Rh complexes were prepared according to slightly modified literature procedures. For more details, see Electronic Supporting Information.

*General experimental procedure for the preparation of Rh-complexes (*Figure 9*):* Inside of the glove box an oven-dried 25 mL round bottom flask was charged with $[Rh(cod)Cl]_2$ (100.0 mg, 1 equiv.) and $AgSbF_6$.The flask was sealed with a rubber septa, removed from the glove box, and equipped with an Ar balloon. Inside of the glove box, another oven dried 25 mL round bottom flask was charged with the corresponding chelating ligand (2 equiv.), sealed with a rubber septum, removed from the glove box, and equipped with an Ar balloon. Both flasks were charged with dry $CHCl_3$ (5 mL) and allowed to stir for 30 min at 20 °C. This was followed by the dropwise addition of $CHCl_3$ solution of the ligand to the stirring solution of $[Rh(cod)Cl]_2$, which was accompanied by precipitation of a white powder (AgCl/NaCl). The resulting mixture was stirred at 20 °C for 1 h. Afterward, the precipitate was filtered off and the solvent was evaporated to give the corresponding complex as an orange powder.

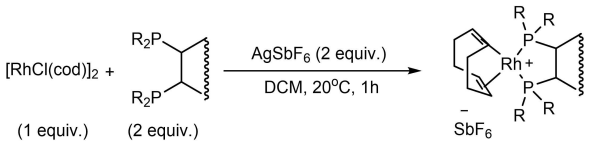

Figure 9. Experimental procedure for the preparation of Rh-complexes.

*General experimental procedure for Rh-catalyzed hydrocarboxylation of ethyl 2-phenylacrylate (*Table 2*):* Inside of the glove box an oven-dried 25 mL Schlenk flask was charged with corresponding Rh-complex (10 mol%) and $AgSbF_6$ (10 mol%). The flask was sealed with a rubber septum, removed from the glove box, evacuated, filled with CO_2 and equipped with a CO_2 balloon. This was followed by sequential addition of dry DMF (5 mL) and ethyl 2-phenylacrylate (150 mg, 1 equiv.) using syringes. The resulting mixture was transferred into an ice bath where under vigorous stirring 1 M solution of Et_2Zn in hexane (1.2 equiv.) was added dropwise using a syringe. The resulting mixture was allowed to stir at 0 °C for 3 h. Then the reaction mixture was diluted with Et_2O (5 mL) and carefully neutralized using 6 M HCl (5 mL). The acidic solution was diluted with water (5 mL) and removed using a separating funnel. The organic phase was then extracted using a solution of saturated $NaHCO_3$ (3 × 30 mL). The collected aqueous solution was carefully treated with 6 M HCl (60 mL) and extracted using Et_2O (3 × 30 mL). Collected Et_2O solution was washed with distilled water (30 mL) and evaporated to give the target acid as a faint orange oil. Enantiomers were separated using SFC on a chiral column (CEL-2), eluent *i*PrOH:EtOH:TFA – 70:30:2, and gradient 3–8, 10 min run.

Starting from 0.851 mmol of ethyl 2-phenylacrylate the product was obtained as a faint orange oil, yield 48%, *e.e.* 32% (0.091 g, [Rh(cod)(((*S*)-SEGPHOS)]SbF_6), yield 74% (0.121 g, [Rh(cod)((*rac*)-StackPhos)]SbF_6), yield 99%, *e.e.* 0% (0.189 g, [Rh(cod)((*S*,*S*)-^{t}Bu-BOX)]SbF_6), yield 94%, *e.e.* 4% (0.178 g, [Rh(cod)((*S*,*S*)-BDPP)]SbF_6). **^{1}H NMR** (400 MHz, $CDCl_3$): δ = 10.38 (br s, 1H), 7.39–7.24 (m, 5H), 4.21 (q, *J* = 7.1 Hz, 2H), 1.87 (s, 3H), 1.22 (t, *J* = 7.1 Hz, 4H). **^{13}C NMR** (101 MHz, $CDCl_3$): δ = 177.0, 171.9, 137.7, 128.4, 128.0, 127.4, 62.3, 58.7, 22.0, 14.0.

Acknowledgements

This work has been supported by the Research Council of Norway (No. 262695, No. 300769), by the Tromsø Research Foundation (No. TFS2016KHH), by Notur – The Norwegian Metacenter for Computational Science through grants of computer time (No. nn9330k and nn4654k), and by NordForsk (No. 85378). We thank Manuel K. Langer for support with the SFC and Prof. Steven Wheeler, Victoria M. Ingman, Anthony J. Schaefer, and Stig Rune Jensen for advice and technical assistance in the implementation of AARON

Conflict of Interest

The authors declare no conflict of interest.

Keywords: Asymmetric catalysis · Carboxylation · Carbon dioxide fixation · Density functional calculations · Rhodium

[1] a) M. Cokoja, C. Bruckmeier, B. Rieger, W. A. Herrmann, F. E. Kühn, *Angew. Chem. Int. Ed. Engl.* **2011**, *50*, 8510–8537; b) S. Dabral, T. Schaub, *Adv. Synth. Catal.* **2019**, *361*, 223–246; c) A. Tortajada, F. Julia-Hernandez, M. Borjesson, T. Moragas, R. Martin, *Angew. Chem. Int. Ed.* **2018**, *57*, 15948–15982; d) Y. Yang, J.-W. Lee, *Chem. Sci.* **2019**, *10*, 3905–3926; e) Y.-X. Luan, M. Ye, *Tetrahedron Lett.* **2018**, *59*, 853–861; f) J. Vaitla, Y. Guttormsen, J. K. Mannisto, A. Nova, T. Repo, A. Bayer, K. H. Hopmann, *ACS Catal.* **2017**, *7*, 7231–7244.
[2] a) T. Fujihara, K. Nogi, T. Xu, J. Terao, Y. Tsuji, *J. Am. Chem. Soc.* **2012**, *134*, 9106–9109; b) T. León, A. Correa, R. Martin, *J. Am. Chem. Soc.* **2013**, *135*, 1221–1224; c) S. Kawashima, K. Aikawa, K. Mikami, *Eur. J. Org. Chem.* **2016**, 3166–3170; d) C. M. Williams, J. B. Johnson, T. Rovis, *J. Am. Chem. Soc.* **2008**, *130*, 14936–14937; e) M. D. Greenhalgh, S. P. Thomas, *J. Am. Chem. Soc.* **2012**, *134*, 11900–11903; f) P. Shao, S. Wang, C. Chen, C. Xi, *Org. Lett.* **2016**, *18*, 2050–2053; g) K. Murata, N. Numasawa, K. Shimomaki, J. Takaya, N. Iwasawa, *Chem. Commun.* **2017**, *53*, 3098–3101; h) M. Juhl, S. L. R. Laursen, Y. Huang, D. U. Nielsen, K. Daasbjerg, T. Skrydstrup, *ACS Catal.* **2017**, *7*, 1392–1396; i) K. Ukai, M. Aoki, J. Takaya, N. Iwasawa, *J. Am. Chem. Soc.* **2006**, *128*, 8706–8707; j) H. Mizuno, J. Takaya, N. Iwasawa, *J. Am. Chem. Soc.* **2011**, *133*, 1251–1253.
[3] a) L. Dian, D. S. Müller, I. Marek, *Angew. Chem. Int. Ed.* **2017**, *56*, 6783–6787; *Angew. Chem.* **2017**, *129*, 6887–6891; b) Y.-Y. Gui, N. Hu, X.-W. Chen, L. L. Liao, T. Ju, J.-H. Ye, Z. Zhang, J. Li, D.-G. Yu, *J. Am. Chem. Soc.* **2017**, *139*, 17011–17014; c) X.-W. Chen, L. Zhu, Y.-Y. Gui, K. Jing, Y.-X. Jiang, Z.-Y. Bo, Y. Lan, J. Li, D.-G. Yu, *J. Am. Chem. Soc.* **2019**, *141*, 18825–18835; d) Y. Shi, B.-W. Pan, Y. Zhou, J. Zhou, Y.-L. Liu, F. Zhou, *Org. Biomol. Chem.* **2020**, *18*, 8597–8619; e) C.-K. Ran, X.-W. Chen, Y.-Y. Gui, J. Liu, L. Song, K. Ren, D.-G. Yu, *Sci. China Chem.* **2020**, *63*, 1336–1351.
[4] Y. G. Liu, Q. Chen, C. L. Mou, L. T. Pan, X. Y. Duan, X. K. Chen, H. Z. Chen, Y. L. Zhao, Y. P. Lu, Z. C. Jin, Y. R. Chi, *Nat. Commun.* **2019**, *10:1675*, 1–8.
[5] Lj. Pavlovic, J. Vaitla, A. Bayer, K. H. Hopmann, *Organometallics* **2018**, *37*, 941–948.
[6] D. García-López, Lj. Pavlovic, K. H. Hopmann, *Organometallics* **2020**, *39*, 1339–1347.
[7] Q. Peng, F. Duarte, R. S. Paton, *Chem. Soc. Rev.* **2016**, *45*, 6093–6107.
[8] a) K. H. Hopmann, *Int. J. Quantum Chem.* **2015**, *115*, 1232–1249; b) H. J. Davis, R. J. Phipps, *Chem. Sci.* **2017**, *8*, 864–877.
[9] a) H. B. Schlegel, *J. Comput. Chem.* **1982**, *3*, 214–218; b) H. B. Schlegel, *Wiley Interdiscip. Rev.: Comput. Mol. Sci.* **2011**, *1*, 790–809; c) J. J. Zheng, M. J. Frisch, *J. Chem. Theory Comput.* **2017**, *13*, 6424–6432; d) C. Gonzalez, H. B. Schlegel, *J. Chem. Phys.* **1989**, *90*, 2154–2161.
[10] a) Y. Guan, V. M. Ingman, B. J. Rooks, S. E. Wheeler, *J. Chem. Theory Comput.* **2018**, *14*, 5249–5261; b) A. R. Rosales, J. Wahlers, E. Limé, R. E. Meadows, K. W. Leslie, R. Savin, F. Bell, E. Hansen, P. Helquist, R. H. Munday, O. Wiest, P.-O. Norrby, *Nat. Can.* **2019**, *2*, 41–45.
[11] a) F. S. P. Cardoso, K. A. Abboud, A. Aponick, *J. Am. Chem. Soc.* **2013**, *135*, 14548–14551; b) P. Braunstein, F. Naud, S. J. Rettig, *New J. Chem.* **2001**, *25*, 32–39; c) B. V. Rokade, P. J. Guiry, *ACS Catal.* **2018**, *8*, 624–643.
[12] G. Desimoni, G. Faita, K. A. Jørgensen, *Chem. Rev.* **2006**, *106*, 3561–3651.
[13] J. Bakos, Á. Orosz, S. Cserépi, I. Tóth, D. Sinou, *J. Mol. Catal. A* **1997**, *116*, 85–97.
[14] a) B. M. Trost, D. L. Van Vranken, *Chem. Rev.* **1996**, *96*, 395–422; b) D. A. Evans, M. M. Faul, M. T. Bilodeau, B. A. Anderson, D. M. Barnes, *J. Am. Chem. Soc.* **1993**, *115*, 5328–5329; c) J. P. Page, T. V. RajanBabu, *J. Am. Chem. Soc.* **2012**, *134*, 6556–6559.
[15] a) H. M. Lee, I. S. Youn, M. Saleh, J. W. Lee, K. S. Kim, *Phys. Chem. Chem. Phys.* **2015**, *17*, 10925–10933; b) E. Hernández-Marín, A. A. Lemus-Santana, *J. Mex. Chem. Soc.* **2015**, *59*, 36–42; c) M. Prakash, K. Mathivon, D. M. Benoit, G. Chambaud, M. Hochlaf, *Phys. Chem. Chem. Phys.* **2014**, *16*, 12503–12509.
[16] D. Kajiya, K.-i. Saitow, *J. Phys. Chem. B* **2010**, *114*, 16832–16837.
[17] P. Li, J. M. Maier, E. C. Vik, C. J. Yehl, B. E. Dial, A. E. Rickher, M. D. Smith, P. J. Pellechia, K. D. Shimizu, *Angew. Chem. Int. Ed. Engl.* **2017**, *56*, 7209–7212.
[18] The costly separation of enantiomers of the synthesized racemic mixture of **L2** was not attempted, due to the computationally predicted low enantiomeric excess expected for this ligand in hydrocarboxylations.
[19] M. J. Frisch, G. W. Trucks, H. B. Schlegel, G. E. Scuseria, M. A. Robb, J. R. Cheeseman, G. Scalmani, V. Barone, B. Mennucci, G. A. Peterson, H. Nakatsuji, M. Caricato, X. Li, H. P. Hratchian, A. F. Izmaylov, J. Bloino, G. Zheng, J. L. Sonnenberg, M. Hada, M. Ehara, K. Toyota, R. Fukuda, J. Hasegawa, M. Ishida, T. Nakajima, Y. Honda, O. Kitao, H. Nakai, T. Vreven, J. A. Jr Montgomery, J. E. Peralta, F. Ogliaro, M. Bearpark, J. J. Heyd, E. Brothers, K. N. Kudin, V. N. Staroverov, R. Kobayashi, J. Normand, K. Raghavachari, A. Rendell, J. C. Burant, S. S. Iyengar, J. Tomasi, M. Cossi, N. Raga, J. M. Millam, M. Klene, J. E. Knox, J. B. Cross, V. Bakken, C. Adamo, J. Jaramillo, R. Gomperts, R. E. Stratmann, O. Yazyev, A. J. Austin, R. Cammi, C. Pomelli, J. W. Ochterski, R. L. Martin, K. Morokuma, V. G. Zakrzewski, G. A. Voth, P. Salvador, J. J. Dannenberg, S. Dapprich, A. D. Daniels, O. Farkas, J. B. Foresman, J. V. Ortiz, J. Cioslowski, D. J. Fox, *Gaussian 09*, *rev. D.01*; Gaussian, Inc., Wallingford, CT, **2013**.
[20] a) A. D. Becke, *Phys. Rev. A* **1988**, *38*, 3098–3100; b) C. Lee, W. Yang, R. G. Parr, *Phys. Rev. B* **1988**, *37*, 785–789.
[21] S. Grimme, *J. Comput. Chem.* **2006**, *27*, 1787–1799.
[22] a) E. Cances, B. Mennucci, J. Tomasi, *J. Chem. Phys.* **1997**, *107*, 3032–3041; b) J. Tomasi, B. Mennucci, E. Cances, *J. Mol. Struct.* **1999**, *464*, 211–226; c) J. Tomasi, B. Mennucci, R. Cammi, *Chem. Rev.* **2005**, *105*, 2999–3094.
[23] R. Krishnan, J. S. Binkley, R. Seeger, J. A. Pople, *J. Chem. Phys.* **1980**, *72*, 650–654.
[24] P. J. Hay, W. R. Wadt, *J. Chem. Phys.* **1985**, *82*, 299–310.
[25] A. W. Ehlers, M. Böhme, S. Dapprich, A. Gobbi, A. Höllwarth, V. Jonas, K. F. Köhler, R. Stegmann, A. Veldkamp, G. Frenking, *Chem. Phys. Lett.* **1993**, *208*, 111–114.
[26] a) C. J. Cramer, *Essentials of computational chemistry: theories and models*, J. Wiley, West Sussex, England; New York, **2002**; b) K. H. Hopmann, *Organometallics* **2016**, *35*, 3795–3807.
[27] S. T. Schneebeli, M. L. Hall, R. Breslow, R. Friesner, *J. Am. Chem. Soc.* **2009**, *131*, 3965–3973.

Manuscript received: November 9, 2020
Revised manuscript received: December 14, 2020
Accepted manuscript online: December 18, 2020